Electronic Supplementary Information for

High effective utilization of ethylene tar for mesophase development via molecular fractionation process

Chuanzhang Ge[a], *Haixiao Yang*[a], *Jitong Wang*[a], *Wenming Qiao*[a,b], *Donghui Long*[a]*, *Licheng Ling*[a]

[a] State Key Laboratory of Chemical Engineering, East China University of Science and Technology, Shanghai 200237, China

[b] Shanghai Key Laboratory of Multiphase Materials Chemical Engineering, Shanghai, China

*Corresponding authors.

E-mail addresses: longdh@mail.ecust.edu.cn

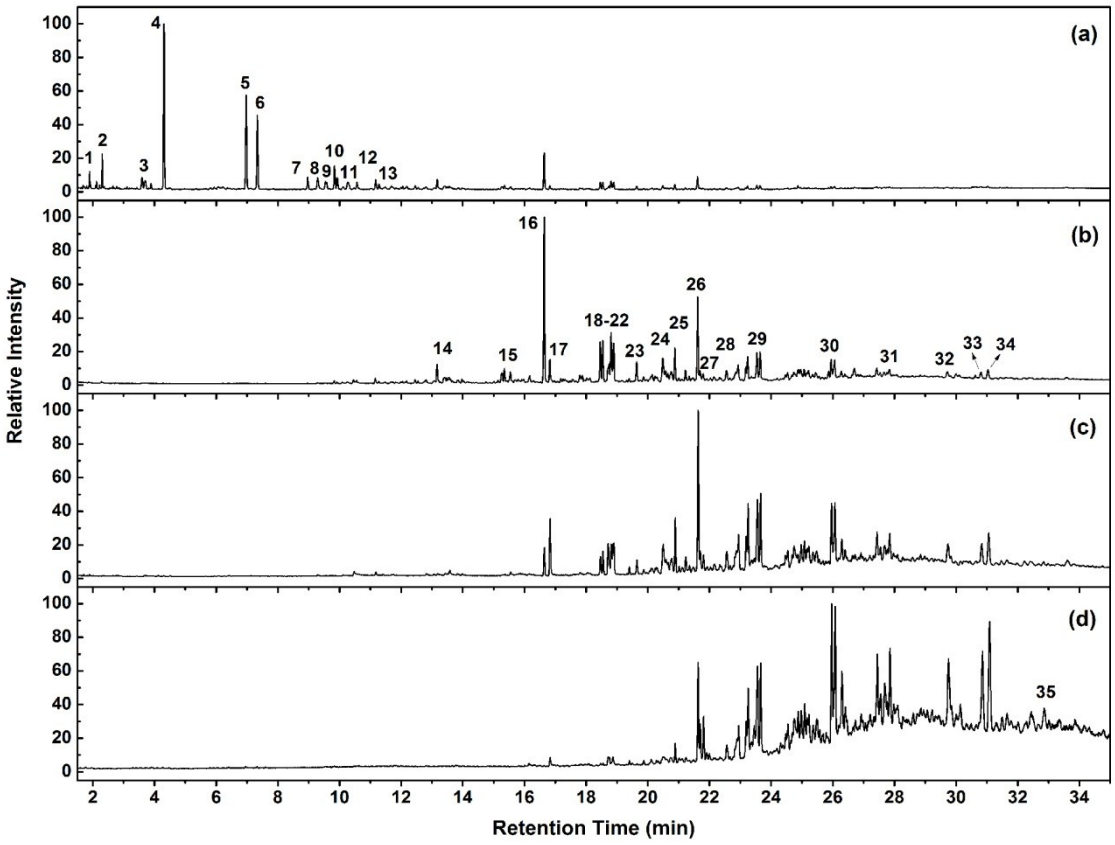

Fig. S1. GC-MS spectrums of (a) ET and heavy residue cutting at (b) 200 °C; (c) 250 °C; (d) 300 °C.

For better classification of the fractions in the ethylene tar and the derived heavy cuts, the main components in these aromatic materials were identified by GC-MS, as shown in Fig. S1. The strong peaks in the spectrums were marked with sequential numbers from the starting retention time to the end. The possible structures corresponding to these peaks were listed in Table S1. It was found that most of the species less than two rings of the molecule were distilled out from the original ET which led to more condensed structure of the heavy residue.

Table S1. Possible components detected by GC-MS in heavy residue of ET

Peak No.	Name or type	Representative structure	Retention time (min)		Area percentage (%)						
			From	To	ET	LF-200	LF-250	LF-300	HC-200	HC-250	HC-300
1	2-Methylstyrene		1.85	1.95	1.59	1.97	1.39	1.49	0	0	0
2	Indene		2.26	2.36	2.98	3.53	2.98	2.95	0	0	0
3	(1-Methyl-1,2-propadienyl)benzene	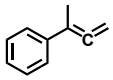	3.53	3.78	4.34	5.80	5.05	5.05	0	0	0
4	Naphthalene		4.22	4.39	23.67	30.45	26.89	23.59	0	0	0
5	2-Methylnaphthalene	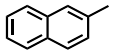	6.88	7.08	14.43	19.70	17.17	15.17	0	0	0
6	1-Methylnaphthalene		7.26	7.43	11.1	15.03	13.36	11.47	0	0	0
7	Bibenzene	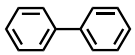	8.89	9.03	1.99	2.40	2.29	1.93	0	0	0
8	1-Ethylnaphthalene		9.22	9.38	2.39	3.28	3.03	2.66	0	0	0
9	2,6-Dimethylnaphthalen	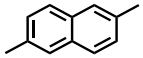	9.49	9.65	1.99	2.85	2.67	2.21	0	0	0

	e										
10	1,7-Dimethylnaphthalene	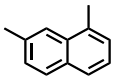	9.79	10.00	5.50	6.98	6.70	5.45	0	0	0
11	2,3-Dimethylnaphthalene	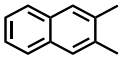	10.20	10.37	2.13	2.67	2.49	2.20	0	0	0
12	1,3-Dimethylnaphthalene	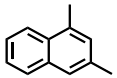	10.52	10.66	1.08	1.35	1.43	1.93	0	0	0
13	Acenaphthene		11.12	11.24	1.54	1.66	1.92	1.77	0	0	0
14	Fluorene	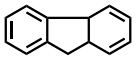	13.10	13.25	1.44	0.98	1.73	1.45	2.01	0	0
15	Methylfluorene	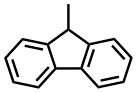	15.19	15.64	2.20	0	2.85	2.10	4.59	0	0
16	Anthracene	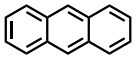	16.56	16.75	5.50	1.37	7.26	5.64	17.17	1.88	0
17	Phenanthrene	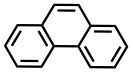	16.75	16.92	0.57	0	0.79	1.07	2.60	5.79	0
18	1-Methylphenanthrene	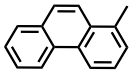	18.37	18.51	1.12	0	0	0	4.32	1.27	0
19	9-Methylanthracene	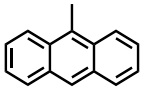	18.51	18.60	1.07	0	0	2.12	4.05	1.52	0

20	Benzo[*def*]fluorene	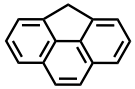	18.65	18.77	0.56	0	0	0	2.82	2.76	0
21	2-Methylphenanthrene	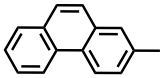	18.77	18.84	0.81	0	0	0	3.48	0.99	0
22	2-Methylanthracene	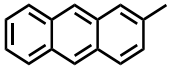	18.84	18.94	1.12	0	0	3.57	4.72	3.73	0
23	2-Phenylnaphthalene	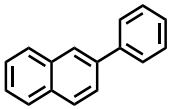	19.56	19.70	0.51	0	0	0.66	2.18	0.96	0
24	Ethylphenanthrene	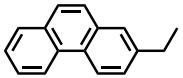	20.40	20.82	2.00	0	0	3.05	9.02	8.29	0
25	Fluoranthene	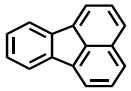	20.82	20.94	0.71	0	0	0	3.41	3.67	0.94
26	Pyrene	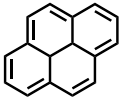	21.52	21.67	1.87	0	0	2.45	9.24	9.76	5.02
27	9-Vinylanthracene	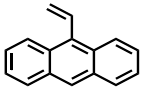	21.74	21.87	0.21	0	0	0	0.73	1.23	1.96
28	2,3-Benzofluorene	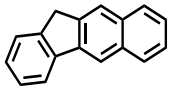	22.49	22.62	0.32	0	0	0	1.40	2.15	1.24

29	Methylpyrene	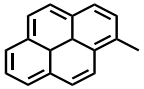	22.71	23.72	2.42	0	0	0	16.18	27.74	29.22
30	Benzanthracene	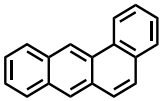	25.89	26.12	0.89	0	0	0	4.47	9.85	15.84
31	Methylchrysene	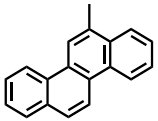	27.33	27.91	0.94	0	0	0	3.56	9.35	18.12
32	Benzo[*e*]pyrene	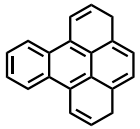	29.63	29.89	0.38	0	0	0	1.45	3.20	8.51
33	Perylene	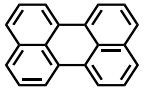	30.73	30.88	0.26	0	0	0	1.04	2.43	7.78
34	Benzo[*b*]fluoranthene	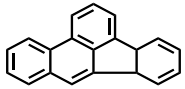	30.94	31.13	0.35	0	0	0	1.58	3.42	9.25
35	13*H*-Dibenzo[*a,h*]fluorene	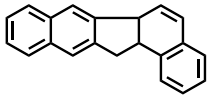	32.76	32.96	0	0	0	0	0	0	2.10

Table S2. Elemental composition of the parent ethylene tar and the derived HCs

Samples	Elemental analysis (wt.%)			C/H[b]
	C	H	O[a]	
ET	92.15	7.20	0.65	1.07
HF-200	93.37	6.29	0.34	1.24
HF-250	93.76	5.94	0.30	1.32
HF-300	94.21	5.51	0.28	1.42

Nitrogen and Sulfur were not found in all of the samples

[a] By difference.

[b] Carbon/hydrogen atomic ratio.

The elemental composition revealed that ET and its derived heavy cuts were almost in absence of N and S which make them suitable precursors for preparation of high performance mesophase pitch. The lower O content of the HCs with respect to that of ET indicated that these distillation cuts are in less hetero-functional groups. The C/H atomic ratio of the HCs was increased with the increasing of distillation temperatures.

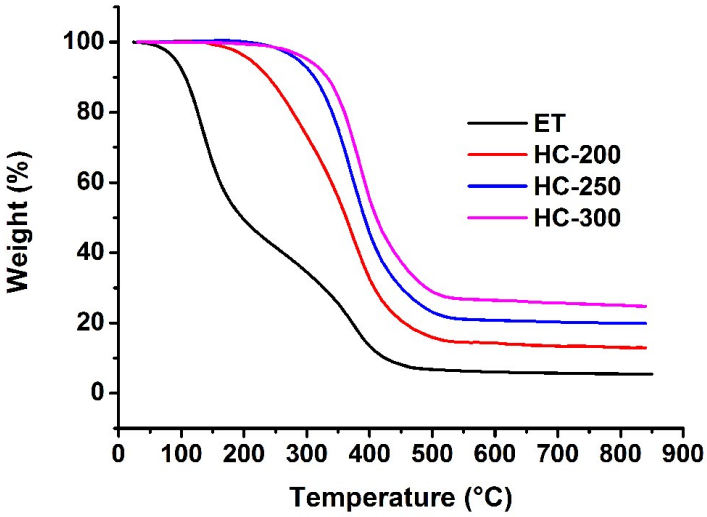

Fig. S2. Thermogravimetric (TG) curves of ET and the derived HCs

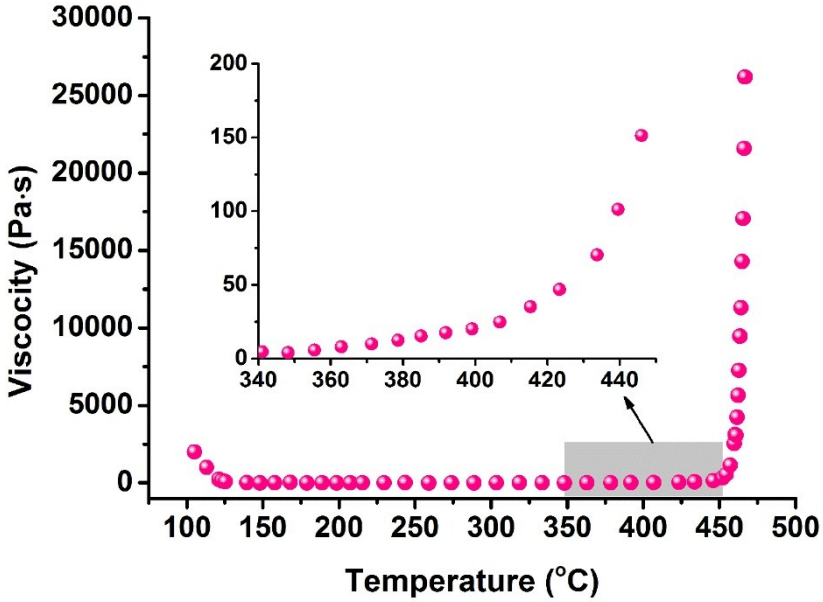

Fig. S3. Viscosity-temperature curve of HC-250

The rheological behavior of HC-250 was studied by high temperature rheometer, as shown in Fig. S3. The viscosity initially decreases with the increasing of temperature and keeps relatively constant between 150 °C and 450 °C, and then sharply increases at temperatures above 450 °C. This sudden increase of the viscosity should be mainly

attributed to the severe volatilization and polymerization of the small molecules. More useful details can be found by careful checking the viscosity curve near the end constant stage, as shown in the inset pattern of Fig. S3. It was noted that the viscosity of the molten HC-250 exhibit a gradual slight increase in the temperature from 360 ^{o}C to 400 ^{o}C, which should be due to the tender polymerization reaction. Such temperature region was an ideal scope for the mesophase pitch preparation. In the light of this result, temperatures of 360 ºC, 380 ºC and 400 ºC were applied for the carbonization of HC-250.

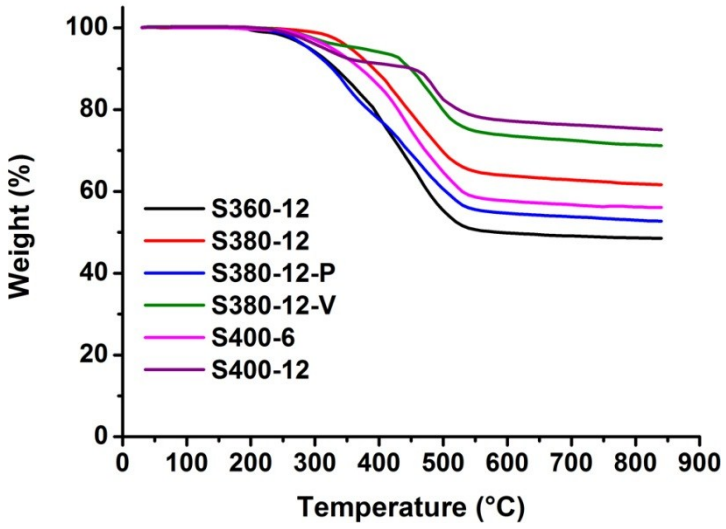

Fig. S4. TG curves of the pitches prepared from HC-250 under different conditions

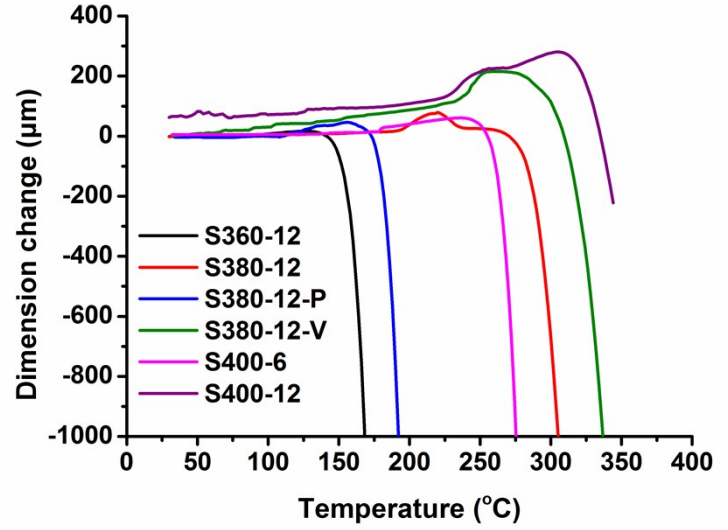

Fig. S5. Thermomechanical (TMA) curves of the prepared pitches

Fig. S5 shows the softening point of the prepared pitch determined by TMA analysis. TMA curve recorded the dimensional change of the pitch samples with the increasing of temperature. The softening point was determined from the intersection of tangents before and after the penetration.